Geomechanics and Engineering, *Vol. 35, No. 4 (2023) 367-383*
https://doi.org/10.12989/gae.2023.35.4.367

Free vibrational behavior of perfect and imperfect multi-directional FG plates and curved structures

Pankaj S. Ghatage[1,2], P. Edwin Sudhagar*[1] and Vishesh R. Kar[3]

[1]*School of Mechanical Engineering, Vellore Institute of Technology, Vellore - 632014, Tamilnadu, India*
[2]*Department of Automobile Engineering, Rajarambapu Institute of Technology, Rajaramnagar, Affiliated to Shivaji University, Kolhapur, Islampur - 415414, Maharashtra, India*
[3]*Department of Mechanical Engineering, National Institute of Technology Jamshedpur, – 831014, India*

(*Received March 26, 2023, Revised September 27, 2023, Accepted October 30, 2023*)

Abstract. The present paper examines the natural frequency responses of the bi-directional (n_x-n_y, n_y-n_z and n_z- n_x) and multi-directional (n_x-n_y-n_z) functionally graded (FG) plate and curved structures with and without porosity. The even and uneven kind of porosity pattern are considered to observe the influence of porosity type and porosity index. The numerical findings have been obtained using a higher order shear deformation theory (HSDT) based isometric finite element (FE) approach generated in a MATLAB platform. According to the convergence and validation investigation, the proposed HSDT based FE model is adequate to predict free vibrational responses of multidirectional porous FG plates and curved structures. Further a parametric analysis is carried out by taking various design parameters into account. The free vibrational behavior of bidirectional (2D) and multidirectional (3D) perfect-imperfect FGM structure is examined against various power law index, support conditions, aspect, and thickness ratio, and for the curvature of curved structures. The results indicate that the maximum non-dimensional fundamental frequency (NFF) value is observed in perfect FGM plates and curved structures compared to porous FGM plates and curved structures and it is maximum for FGM plates and curved structures with uneven kind of porosity than even porosity.

Keywords: FEM; free vibration; functionally graded materials; plates and curved structures; porosity

1. Introduction

Recently, some researchers proved that multidirectional functionally graded composite materials have great potential to develop and optimise structures under multifunctional requirements Mehrabadi and Aragh (2013), which results in attracting considerable attention in field of engineering because of their enormous advantages over conventional laminated composites and unidirectional functionally graded materials (FGMs). Hence, FGMs are being utilized in the field of engineering to design different structures and structural components because of their potential functions. The plates and curved structures play a significant role in the engineering structures and components, as these geometrical shapes provide better strength and stability to the structures with good aesthetics and ergonomics which motivates the designer to select such geometries. However, the vibration behaviour of such structures needs to be obtained for better design and safety, because undesirable vibrations may hamper the structural integrity of the product. To predict the vibration behaviour of such structures experimentally is time consuming and expensive, hence many researchers predicted the vibration behaviour of FGMs with analytical and numerical methods. Some of the relevant literature is discussed in the following.

Pradyumna and Bandyopadhyay (2008) presented a vibrational behavior of unidirectional (1D) FG curved structures, including cylindrical shells using higher-order FEM approach. Tornabene (2009) conducted free vibrational investigation of 1D FG conical and cylindrical shell based on first order shear deformation theory (FSDT). Tornabene *et al.* (2009) carried out a vibrational analysis of 1D FG conical and cylindrical shell along with annular plate structure using FSDT, and the computed results were validated by comparing the results obtained from different commercial software. Punera and Kant (2017) investigated the free vibrational behavior of 1D FG cylindrical shells based on higher-order shear and normal deformation theory (HOSNT), FSDT and HSDT models. Kar and Panda (2015) presented a free vibrational behavior of FG curved structures in a thermal medium using HSDT. Free vibration and buckling analysis of double-porous FG nanoplates using quasi-3D refined theory presented by Sobhy and Zenkour (2019). Khiloun *et al.* (2020) analysed the free vibrational and bending behavior of 1D thick FG plates using simple plate theory with four unknowns. Bansal *et al.* (2020) presented the impact of porosity and the geometrical discontinuities on the vibrational behavior of 1D-FG plates. Al Rjoub and Alshatnawi (2020) presented an effect of even type of porosity pattern on the vibrational behavior of 1D porous FG cracked plates. Sayyad and Ghugal (2021) studied the static and vibrational behaviour of FG shell structure with various single layer shell theory. Kang *et al.* (2022) studied the free vibrational behavior of FG plates at distinct boundary conditions in thermal environment. The

*Corresponding author, Associate Professor,
E-mail: edwinsudhagar.p@vit.ac.in

ISSN: 2005-307X (Print), 2092-6219 (Online)

free vibration analysis of unidirectional FG thick plates and micro-nano plates using 3D elasticity theory studied by a group of researchers (Hosseini-Hashemi *et al.* 2013, Salehipour *et al.* 2015, Salehipour and Shahsavar 2018).

The literatures previously mentioned was only limited to 1D FGMs, to fulfil the demand of some engineering and aerospace applications, researchers extended the work to bi-directional (2D) FGMs (Nemat-Alla 2003). Ebrahimi and Najafizadeh (2014) presented the comparative study of vibrational responses of 2D-FG cylindrical shell and 1D-FG cylindrical shell based on love's first approximation classical shell theory. Tahouneh and Naei (2016) proved that the 2D-FG composites has the ability to reduce natural frequency compared to 1D-FG composites. Lieu *et al.* (2018) presented a flexural and vibrational behavior of in-plane 2D-FG plates considering inconstant thickness. Ahlawat and Lal (2016) studied the buckling and vibration analysis of 2D- FG circular plates. Ghatage *et al.* (2020) have presented the first time, a review of multidirectional FG composite structures including its modelling and analysis. Wu and Yu (2019) analyzed the free vibrational behavior of 2D-FG plates with the help of a finite annular prism method, the impact of different support conditions on free vibrational behavior of plates were studied. Chen *et al.* (2018) proposed FSDT and a typical isogeometric analysis (IGA) for 2D-FG sector cylindrical shells to investigate natural frequency. Molla-Alipour *et al.* (2020) presented free vibrational behavior of 2D-FG cylindrical, conical shells and annular plates using nonlinear elastic foundation using unified formulation. Cuong-Le *et al.* (2021) studied the effect of size parameters on natural frequency and critical buckling of 2D-FG nano-shells using 3D-IGA approach.

During the manufacturing process of FGMs, porosities are formed. Hence many studies of 1D-FGM considering the even and uneven porosity reported recently. However the research literature on 2D-FGM with porosity is still very limited. Esmaeilzadeh and Kadkhodayan (2019) studied a dynamic analysis of porous 2D-FGM plates using a dynamic relaxation method. Bathini (2020) studied the free vibration behavior of imperfect 2D-FG plates using refined FSDT and discussed the effect of different parameters on vibrational behavior of 2D-FG plates. Li *et al.* (2020) applied IGA and FSDT to study free vibration, bending and buckling behavior of imperfect 2D-FG plates. Ramteke and Panda (2021) presented the free vibration behavior of 2D porous FGM structures considering even and uneven porosity pattern. These authors went one step further and used HSDT to evaluate the nonlinear frequency of porous 2D-FG doubly curved shell structures (Ramteke *et al.* 2022). Sah and Ghosh, (2022) presented the impact of porosity on vibration and buckling behavior 2D-FGM sandwich plates using sinusoidal shear deformation theory.

The free vibrational behavior of bidirectional FG plates and shell with and without porosity was studied by Ghatage and Sudhagar (2023a, 2023b). Due to applications of macro-micro-nano FGM structures in electromechanical industries, many researchers studied the free vibrational behavior of porous macro-micro-nano FGM structures (Talebizadehsardari *et al.* 2020, Salehipour *et al.* 2019, Salehipour *et al.* 2020).

Literature study shows that a lot of research has been reported on the vibration analysis of FGMs to get effective performance in required applications. It should be observed that the studies discussed above are restricted to FGMs with no porosity, and research on porous FGMs is still in its early stages. During the study, authors considered unidirectional FGM plates and curved structures, and very few studies were focused on the bi-directional or multi-directional FGM plates and curved structures (Şimşek 2015). Hence, in the present work, a computational model is developed to predict the free vibrational behavior of bi-directional and multi-directional perfect and porous FG plates and curved structures utilizing HSDT in conjunction with FEM. Convergence and validation studies are performed on the developed computational model to ensure its accuracy and effectiveness. Additionally, a parametric study is conducted to present the effect of grading patterns, thickness and aspect ratio, curvature ratio, shapes of geometry, support conditions, porosity type on dimensionless frequencies of multidirectional FG plates and curved structures by different illustrations.

2. Mathematical modelling

The present paper examines the eigen frequency properties of the FG plates and curved structures, for the analysis of the FG structures, various material grading schemes and porous variations are used.

In section 3.1 FGM with the grading of material properties in two directions is considered along (*x-y*), (*y-z*), and (*x-z*) directions, that is bidirectional property variations. Section 3.2 considers variation in material properties in three directions (3D) along (*x-y-z*) directions, which makes the study unique.

First, by considering material grading along the (*x, y*), (*y, z*), and (*x, z*) directions, the effective material properties of FGM are obtained. A Voigt's micromechanical model is employed in conjunction with the volume fraction of the materials to produce this elastic property fluctuation. Elastic property (*EP*) variation in multidirectional can be written as in Eq. (1) (Kar and Panda 2015b)

$$EP = [EP_c - EP_m]V_c + EP_m \tag{1}$$

Where c and m suffix stand for ceramic and metal. V_c defines the volume fraction of ceramic, which can be expressed as

$$\begin{gathered} V_c = \left(\frac{1}{2} + \frac{\varrho}{h}\right)^{n_z} \left(\frac{\jmath}{a}\right)^{n_x} and\, V_m = 1 - V_c \\ V_c = \left(\frac{1}{2} + \frac{\varrho}{h}\right)^{n_z} \left(\frac{\jmath}{a}\right)^{n_x} \left(\frac{\varsigma}{b}\right)^{n_y} and\, V_m = 1 - V_c \end{gathered} \tag{2}$$

In above expression $\jmath$, ς and ϱ are any arbitrary point of consideration along $x, y,$ and z directions. Further expression (1) can be written for considering porosity (either even or uneven) as Eqs. (3) and (4) (Hadji *et al.* 2021, Keddouri *et al.* 2019, Ramteke *et al.* 2022, Ramteke and Panda 2021)

$$EP = EP_{mc}V_c + EP_m - 0.5\alpha\,(EP_c + EP_m) \tag{3}$$

$$EP = EP_{mc}V_c + EP_m - 0.5\alpha\,(EP_c + EP_m)\left(1 - \frac{2|\varrho|}{h}\right), \tag{4}$$

α=porocity index

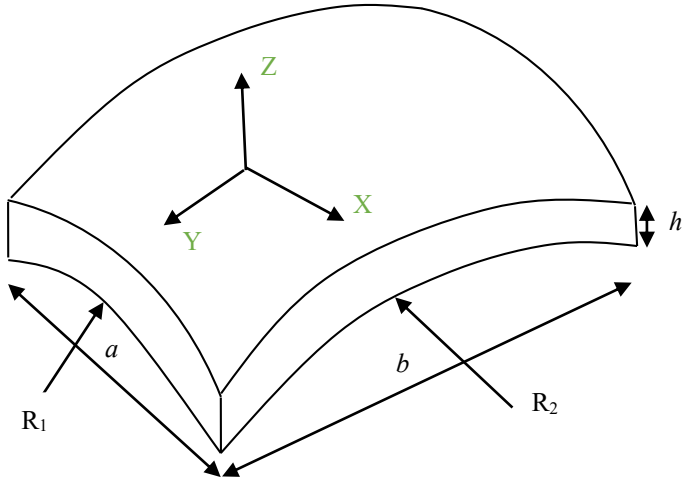

Fig. 1 Geometry of FGM panel

Table 1 Distinct FGM plate and curved structures

Curvature Radii	FGM Structures				
	Plate	Cylindrical	Spherical	Elliptical	Hyperbolic
R_1	∞	R	R	R	R
R_2	∞	∞	R	2R	-R

Eq. (3) shows an even type of porosity distribution and Eq. (4) shows an uneven type of porosity distribution. The geometry of the curved FGM panel is shown in Fig. 1, where R_1 *and* R_2 shows the radius of curvature, h is the thickness in z direction, side a and b are in the x and y directions respectively. The plate and distinct curved structures can be defined in terms of radius of curvature is depicted in Table 1.

The HSDT formulation is used to predict the free vibration behavior of multidirectional FGM plates and curved structures in this work, the displacement field of multidirectional FG structures is modelled utilizing HSDT with nine degrees of freedom are supposed to be in Eq. (5) (Kar and Panda 2015a, b, 2016)

$$\begin{pmatrix} u \\ v \\ w \end{pmatrix} = \begin{bmatrix} 1 & 0 & 0 & z & 0 & z^2 & 0 & z^3 & 0 \\ 0 & 1 & 0 & 0 & z & 0 & z^2 & 0 & z^3 \\ 0 & 0 & 1 & 0 & 0 & 0 & 0 & 0 & 0 \end{bmatrix} \begin{pmatrix} u_{00} \\ v_{00} \\ w_{00} \\ \phi_x \\ \phi_y \\ u_0^{\bullet} \\ v_0^{\bullet} \\ \theta_x^{\bullet} \\ \theta_y^{\bullet} \end{pmatrix} \tag{5}$$

$$\{\lambda\} = [f]\{\lambda_0\} \tag{6}$$

Where, u_{00}, v_{00} and w_{00} are the midplane displacements along the x, y and z directions respectively. ϕ_x and ϕ_y represents the shear rotation along the x-axis and y-axis respectively. $(u_0^{\bullet}, v_0^{\bullet}, \theta_x^{\bullet}, \theta_y^{\bullet})$ are the higher-order terms. $[f]$ represents the function of thickness coordinate. The global displacements $\{\lambda\} = \lfloor u\ v\ w \rfloor^T$ (u, v, w) at any point along (x, y, z) directions in the structure are presented in terms of mid-plane displacements $\{\lambda_0\} = \lfloor u_0\ v_0\ w_0\ \phi_x\ \phi_y\ u_o^{\bullet}\ v_o^{\bullet}\ \theta_x^{\bullet}\ \theta_y^{\bullet} \rfloor^T$ as in Eq. (5).

The strain tensor $\varepsilon = \lfloor \varepsilon_{xx}\ \varepsilon_{yy}\ \varepsilon_{xy}\ \varepsilon_{xz}\ \varepsilon_{yz} \rfloor^T$ of multidirectional FGM is given as in Eqn. (3.36).

$$\begin{Bmatrix} \varepsilon_{xx} \\ \varepsilon_{yy} \\ \varepsilon_{xy} \\ \varepsilon_{xz} \\ \varepsilon_{yz} \end{Bmatrix} = \begin{bmatrix} \dfrac{\partial u}{\partial x} \\ \dfrac{\partial v}{\partial y} \\ \dfrac{1}{2}\left(\dfrac{\partial u}{\partial y} + \dfrac{\partial v}{\partial x}\right) \\ \dfrac{1}{2}\left(\dfrac{\partial u}{\partial z} + \dfrac{\partial w}{\partial x}\right) \\ \dfrac{1}{2}\left(\dfrac{\partial v}{\partial z} + \dfrac{\partial w}{\partial y}\right) \end{bmatrix} \tag{7}$$

Now, substituting the displacements as in Eq. (1) into Eq. (7), the strain terms can be represented as

$$\begin{Bmatrix} \varepsilon_{xx} \\ \varepsilon_{yy} \\ \gamma_{xy} \\ \gamma_{xz} \\ \gamma_{yz} \end{Bmatrix} = \begin{Bmatrix} \varepsilon_x^0 \\ \varepsilon_y^0 \\ \varepsilon_{xy}^0 \\ \varepsilon_{xz}^0 \\ \varepsilon_{yz}^0 \end{Bmatrix} + z \begin{Bmatrix} k_x^1 \\ k_y^1 \\ k_{xy}^1 \\ k_{xz}^1 \\ k_{yz}^1 \end{Bmatrix} + z^2 \begin{Bmatrix} k_x^2 \\ k_y^2 \\ k_{xy}^2 \\ k_{xz}^2 \\ k_{yz}^2 \end{Bmatrix} + z^3 \begin{Bmatrix} k_x^3 \\ k_y^3 \\ k_{xy}^3 \\ k_{xz}^3 \\ k_{yz}^3 \end{Bmatrix} \tag{8}$$

The strain tensor $\{\varepsilon\}$ can be expressed in terms of strain vectors $\{\bar{\varepsilon}\}$ and thickness coordinate matrix $[T]$ as

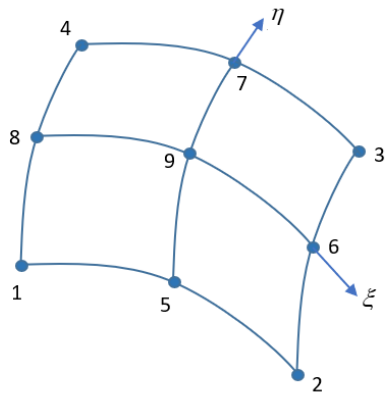

Fig. 2 A 9-node quadrilateral Lagrangian 2D element

shown in Eq. (9)

$$\{\varepsilon\}=[T]\{\bar{\varepsilon}\} \tag{9}$$

where

$$\{\bar{\varepsilon}\}=\left[\varepsilon_x^0\ \varepsilon_y^0\ \varepsilon_{xy}^0\ \varepsilon_{xz}^0\ \varepsilon_{yz}^0\ k_x^1\ k_y^1\ k_{xy}^1\ k_{xz}^1\ k_{yz}^1\ k_x^2\ k_y^2\ k_{xy}^2\ k_{xz}^2\ k_{yz}^2\ k_x^3\ k_y^3\ k_{xy}^3\ k_{xz}^3\ k_{yz}^3\right]^T \tag{10}$$

In the above equation, the terms with superscripts 0, 1-3 are membrane and higher order mid-plane strain terms respectively and can be expressed as Eq. (11)

$$\left.\begin{aligned}
&\varepsilon_x^0=u_x,\ \varepsilon_y^0=v_y,\ \varepsilon_{xy}^0=u_y+v_x,\ \varepsilon_{xz}^0=w_x+\phi_x,\ \varepsilon_{yz}^0=w_y+\phi_y;\\
&k_x^1=\phi_{x,x},\ k_y^1=\phi_{y,y},\ k_{xy}^1=\phi_{x,y}+\phi_{y,x},\ k_{xz}^1=2u_0^{\bullet},\ k_{yz}^1=2v_0^{\bullet};\\
&k_x^2=u_{0,x}^{\bullet},\ k_y^2=v_{0,y}^{\bullet},\ k_{xy}^2=u_{0,y}^{\bullet}+v_{0,x}^{\bullet},\ k_{xz}^2=3\theta_x^{\bullet},\ k_{yz}^2=3\theta_y^{\bullet};\\
&k_x^3=\theta_{x,x}^{\bullet},\ k_y^3=\theta_{y,y}^{\bullet},\ k_{xy}^3=\theta_{x,y}^{\bullet}+\theta_{y,x}^{\bullet}
\end{aligned}\right\} \tag{11}$$

The constitutive relations may be expressed as in Eq. (12)

$$\begin{Bmatrix}\sigma_{xx}\\ \sigma_{yy}\\ \sigma_{xy}\\ \sigma_{xz}\\ \sigma_{yz}\end{Bmatrix}=\begin{bmatrix}C_{11}&C_{12}&0&0&0\\ C_{21}&C_{22}&0&0&0\\ 0&0&C_{33}&0&0\\ 0&0&0&C_{44}&0\\ 0&0&0&0&C_{55}\end{bmatrix}\begin{Bmatrix}\varepsilon_{xx}\\ \varepsilon_{yy}\\ \varepsilon_{xy}\\ \varepsilon_{xz}\\ \varepsilon_{yz}\end{Bmatrix} \tag{12}$$

Where,

$$C_{11}=C_{22}=\frac{E_{(x,y,z)}}{1-\upsilon^2_{(x,y,z)}},C_{12}=C_{21}=\frac{\upsilon E_{(x,y,z)}}{1-\upsilon^2_{(x,y,z)}},C_{33}=C_{44}=C_{55}=\frac{E_{(x,y,z)}}{2\left(1+\upsilon_{(x,y,z)}\right)}$$

The Eqn. (12) can be expressed as per Eq. (13)

$$\{\sigma\}=[C]\{\varepsilon\} \tag{13}$$

where, $\{\sigma\}$ is the stress tensor, $\{\varepsilon\}$ is the strain tensor and thermal strain tensor respectively. $[C]$ represents stiffness matrix

A generic governing equation for the current higher-order model is derived using Hamilton's principle, which is expressed in Eq. (14)

$$\delta\int_{t_1}^{t_2}\left(U_k-U_s\right)dt=0 \tag{14}$$

Here, strain energy $\left(U_s\right)$ can be provided in Eq. (15)

$$\begin{aligned}U_s&=\frac{1}{2}\int\left(\int_{-h/2}^{+h/2}\{\varepsilon\}^T[C]\{\varepsilon\}\,dz\right)dA\\&=\frac{1}{2}\int_A\left(\{\bar{\varepsilon}\}^T[R]\{\bar{\varepsilon}\}\right)dA\end{aligned} \tag{15}$$

Here, kinetic energy $\left(U_k\right)$ can be provided in Eq. (16)

$$\begin{aligned}U_k&=\frac{1}{2}\int_A\left(\int_{-h/2}^{+h/2}\rho(x,y)\left(\dot{u}^2+\dot{v}^2+\dot{w}^2\right)dz\right)dA\\&=\frac{1}{2}\int_A\left(\int_{-h/2}^{+h/2}\{\dot{\lambda}_0\}^T[f]^T\rho[f]\{\dot{\lambda}_0\}\,dz\right)dA\\&=\frac{1}{2}\int_A\{\dot{\lambda}_0\}^T[m]\{\dot{\lambda}_0\}\,dA\end{aligned} \tag{16}$$

where

$$[R]=\begin{bmatrix}R_1&R_2&R_3&R_4\\ R_2&R_3&R_4&R_5\\ R_3&R_4&R_5&R_6\\ R_4&R_5&R_6&R_7\end{bmatrix} \tag{17}$$

$$\left(R_1,R_2,R_3,R_4,R_5,R_6,R_7\right)_{ij}=\int_{-h/2}^{h/2}C(x,y)\left(1,z,z^2,z^3,z^4,z^5,z^6\right)dz\quad\{i,j=1,2,6,5,4\} \tag{18}$$

$$[m]=\begin{bmatrix}I_1&0&0&I_2&0&I_3&0&I_4&0\\ 0&I_1&0&0&I_2&0&I_3&0&I_4\\ 0&0&I_1&0&0&0&0&0&0\\ I_2&0&0&I_3&0&I_4&0&I_5&0\\ 0&I_2&0&0&I_3&0&I_4&0&I_5\\ I_3&0&0&I_4&0&I_5&0&I_6&0\\ 0&I_3&0&0&I_4&0&I_5&0&I_6\\ I_4&0&0&I_5&0&I_6&0&I_7&0\\ 0&I_4&0&0&I_5&0&I_6&0&I_7\end{bmatrix} \tag{19}$$

$$\left(I_1,I_2,I_3,I_4,I_5,I_6,I_7\right)=\int_{-h/2}^{h/2}\rho(x,y)\left(1,z,z^2,z^3,z^4,z^5,z^6\right)dz \tag{20}$$

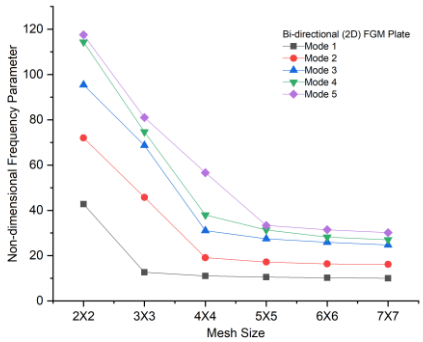

Fig. 3 Convergence study of bi-directional perfect FGM plate

Further, 2D isoparametric FEM technique is adopted to get the system of algebraic equations from Eq. (14). For this purpose, nine nodes quadrilateral Lagrangian elements are utilized, which is depicted in Fig. 2. For any element, the displacement vector can be now expressed in nodal (i = 1, 2, 3,….9) form using shape function N, as in Eq. (21)

$$\begin{pmatrix} u_{00} \\ v_{00} \\ w_{00} \\ \phi_x \\ \phi_y \\ u_0^{\bullet} \\ v_0^{\bullet} \\ \theta_x^{\bullet} \\ \theta_y^{\bullet} \end{pmatrix} = \sum_{i=1}^{9} N_i \begin{pmatrix} u_{00_i} \\ v_{00_i} \\ w_{00_i} \\ \phi_{x_i} \\ \phi_{y_i} \\ u_{0_i}^{\bullet} \\ v_{0_i}^{\bullet} \\ \theta_{x_i}^{\bullet} \\ \theta_{y_i}^{\bullet} \end{pmatrix} \tag{21}$$

where, $\{\lambda_{0_i}\} = \left[u_{00_i}\ v_{00_i}\ w_{00_i}\ \theta_{x_i}\ \theta_{y_i}\ u_{o_i}^{\bullet}\ v_{o_i}^{\bullet}\ \theta_{x_i}^{\bullet}\ \theta_{y_i}^{\bullet}\right]^T$ represents the nodal displacement vector at node i. Now, by imposing Eq. (22) into equation (14), the FEM equation is represented as

$$[K]\lambda + [M]\ddot{\lambda} = 0 \tag{22}$$

where, $[M]^e = \int_{-1}^{1}\int_{-1}^{1} [N]^T[m][N]|J|d\xi d\eta$ represents the mass matrix of element. $[K]^e = \int_{-1}^{1}\int_{-1}^{1} [L]^T[R][L]|J|d\xi d\eta$ represents the stiffness matrix of element. Here, $[L]$ comprises differential operators and shape functions. By substituting $\lambda(x,y,z,t) = \bar{\lambda}(x,y,z,t)e^{i\omega t}$ in Eq. (22), eigenequation of the present 2D-FEM model is given, as

$$\left([K] - \omega^2[M]\right)\{\bar{\lambda}\} = 0 \tag{23}$$

In the En. (23), ω represents the natural frequency and $\bar{\lambda}$ is the mode shape.

The necessary support conditions are considered to restrict the rigid body motion of multidirectional FG plates and curved structures, which are expressed in Eq. (24) to (27).

Fully clamped (CCCC)

$$u_{00} = v_{00} = w_{00} = \phi_x = \phi_y = u_0^{\bullet} = v_0^{\bullet} = \theta_x^{\bullet} = \theta_y^{\bullet} = 0 \text{ at } x = 0, a \text{ and } y = 0, b \tag{24}$$

Fully simply supported (SSSS)

$$\begin{aligned} v_{00} = w_{00} = \phi_y = v_0^{\bullet} = \theta_y^{\bullet} = 0 \text{ at } x = 0, a \\ u_{00} = w_{00} = \phi_x = u_0^{\bullet} = \theta_x^{\bullet} = 0 \text{ at } y = 0, b \end{aligned} \tag{25}$$

Clamped/Simply supported (SCSC)

$$\begin{aligned} v_{00} = w_{00} = \phi_y = v_0^{\bullet} = \theta_y^{\bullet} = 0 \text{ at } x = 0, a \text{ and} \\ u_{00} = v_{00} = w_{00} = \phi_x = \phi_y = u_0^{\bullet} = v_0^{\bullet} = \theta_x^{\bullet} = \theta_y^{\bullet} = 0 \text{ at } y = 0, b \end{aligned} \tag{26}$$

Cantilever (CFFF)

$$u_{00} = v_{00} = w_{00} = \phi_x = \phi_y = u_0^{\bullet} = v_0^{\bullet} = \theta_x^{\bullet} = \theta_y^{\bullet} = 0 \text{ at } y = 0 \tag{27}$$

3. Results and discussions

The FGMs are designed especially for applications in the fields of aerospace, automobile, military, and so on, where the FGM structures are exposed to a variety of complex environments. As a result, to assure the safety of such structures, the natural frequency of the FGM structures must be anticipated in order to avoid resonance. In the current study, a MATLAB code is created to predict characteristics of free vibration of bidirectional and multidirectional FGM plates and curved structures using a finite element approach based on HSDT. This section will first execute a convergence and validation study to demonstrate the stability of the MATLAB code and then validate the research's findings to demonstrate the accuracy of the results with respect to several design-dependent characteristics. Further, the influence of distinct parameters on free vibration behavior of perfect and porous multidirectional FG plates and curved structures is presented. Unless otherwise stated, the following lists the material parameters and other input factors used in this study:

Si_3N_4 : $E_c = 348.43\ GPa, \mu_c = 0.3, \rho_c = 2370\ kg/m^3$

$SUS304$: $E_m = 201.04\ GPa, \mu_c = 0.3, \rho_c = 8166\ kg/m^3$

3.1 Convergence and validation study

A convergence study is needed in order to use FEM to obtain the appropriate and accurate results. So, in this study,

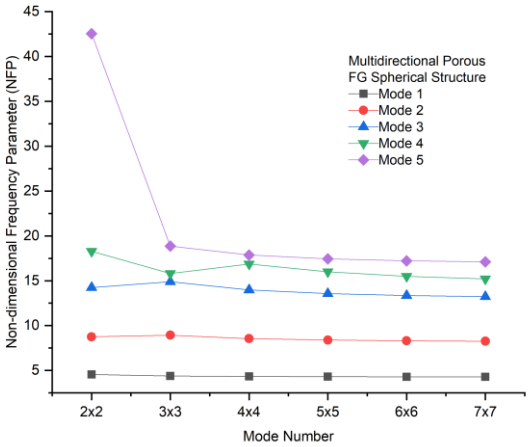

Fig. 4 Convergence study of multidirectional porous FGM spherical structure

Table 2 Non-dimensional fundamental frequency for 2D-FG plate with a/h = 10

Power law index		Present HSDT (2D-FEM)	Lieu *et al.* (2019)	% Difference
n_y	n_x			
0	0	3.4152	3.3367	2.2985
	0.5	2.3677	2.2832	3.5689
	1	1.9890	1.931	2.9160
	2	1.6956	1.6625	1.9521
	5	1.4907	1.4780	0.8519
	10	1.4329	1.4299	0.2094
0.5	0	2.3677	2.2834	3.5604
	0.5	1.9708	1.9026	3.4605
	1	1.7760	1.7278	2.7140
	2	1.6005	1.5713	1.8244
	5	1.4634	1.4507	0.8678
	10	1.4225	1.4177	0.3374
1	0	1.9890	1.9311	2.9110
	0.5	1.7760	1.7278	2.7140
	1	1.6585	1.6225	2.1706
	2	1.5433	1.5196	1.5357
	5	1.4461	1.4343	0.8160
	10	1.4159	1.4100	0.4167
2	0	1.6956	1.6625	1.9521
	0.5	1.6005	1.5713	1.8244
	1	1.5433	1.5196	1.5357
	2	1.4824	1.4696	0.8635
	5	1.4265	1.4158	0.7501
	10	1.4084	1.4013	0.5041
5	0	1.4907	1.4780	0.8519
	0.5	1.4634	1.4507	0.8678
	1	1.4461	1.4342	0.8229
	2	1.4265	1.4158	0.7501
	5	1.4074	1.3983	0.6466
	10	1.4011	1.393	0.5781
10	0	1.4329	1.4299	0.2094
	0.5	1.4225	1.4176	0.3445
	1	1.4159	1.4100	0.4167
	2	1.4084	1.4013	0.5041
	5	1.4011	1.393	0.5781
	10	1.3987	1.3906	0.5791

Table 3 Non-dimensional fundamental frequency for 2D-FG plate with a/h = 50

Power law index		Present HSDT	Lieu *et al.* (2019)	% Difference
n_y	n_x			
0	0	3.4764	3.3611	3.3166
	0.5	2.5745	2.4996	2.9093
	1	2.2305	2.1180	5.0437
	2	1.9786	1.8235	7.8389
	5	1.7318	1.6207	6.4153
	10	1.6649	1.5691	5.7541
0.5	0	2.6745	2.4996	6.5395
	0.5	2.2076	2.0850	5.5535
	1	2.0068	1.8949	5.5760
	2	1.8657	1.7233	7.6325
	5	1.7007	1.5911	6.4444
	10	1.6536	1.5558	5.9144
1	0	2.2305	2.1180	5.0437
	0.5	2.0768	1.8949	8.7587
	1	1.9365	1.7797	8.0971
	2	1.7976	1.6668	7.2764
	5	1.6810	1.5733	6.4069
	10	1.6465	1.5474	6.0188
2	0	1.9786	1.8235	7.8389
	0.5	1.8657	1.7233	7.6325
	1	1.7976	1.6668	7.2764
	2	1.7249	1.6069	6.8410
	5	1.6589	1.5534	6.3596
	10	1.6385	1.5380	6.1337
5	0	1.7318	1.6207	6.4153
	0.5	1.7007	1.5911	6.4444
	1	1.6810	1.5733	6.4069
	2	1.6589	1.5534	6.3596
	5	1.6376	1.5346	6.2897
	10	1.6308	1.529	6.2423
10	0	1.6649	1.5691	5.7541
	0.5	1.6536	1.5558	5.9144
	1	1.6465	1.5474	6.0188
	2	1.6385	1.5380	6.1337
	5	1.6308	1.5290	6.2423
	10	1.6284	1.5264	6.2638

the convergence behavior of the developed model is demonstrated by two different illustrations. Fig. 3 show that, a convergence behavior of bi-directional (Power law index: n_x = 0.5, n_z = 1) perfect FG plates. For the study FGM (*SUS304 and Si_3N_4*) plate with aspect ratio 1.5, thickness ratio 50 under all side clamped boundary conditions is utilized. The non-dimensional frequency parameters of bi-directional and multi-directional perfect FG plates for the first five modes with different mesh size are plotted. The study demonstrates that results from a mesh size of 5×5 components of NFP modes are steady, and little change is seen after a certain point mesh size with 5×5 elements. Hence, the 25 element is sufficient to compute the free vibrational responses of the multidirectional perfect FG structures.

The convergence behavior of the multidirectional FG spherical structure with even kind of porosity is shown in Fig. 4. The FG (SUS304 and Si_3N_4) spherical structure is used in this work, with fully simply supported (*SSSS*) boundary condition, thickness ratio (a/h) 50, aspect ratio (a/b) 1.5, curvature ratio (R/a) 50, power-law index: n_x = 0.5, n_y = 0.5, n_z = 1 and porosity index (α) 0.2. The non-dimensional frequencies for the first five modes with different mesh size are computed. It is noticed from all the examples that, the mesh size (5×5) is shown to be appropriate for analyzing the free vibrational behavior of multidirectional FG curved structures with porosity.

Tables 2 and 3 shows the evaluation of nondimensional fundamental frequency of square FGM under all side clamped boundary condition and thickness ratio (a/h) of 10 and 50. Nondimensional fundamental frequency were evaluated by

$$\bar{\omega} = \omega(a/\pi)^2\sqrt{12\,\rho_c(1-\nu_c^2)/E_c h^2}$$

The FGM plate considered is of bi-directional material property variation. For the various values of n_x *and* n_y, NFF is found and the obtained results are compared with the literature results of Lieu *et al.* (2019). It is observed that the result obtained from the presently utilized model are having very close validation with the results from the literature. The average percentage difference is 1.38% and 6.30% for 2D-FG plate with a/h = 10 and a/h = 50. So, for the further study of multidirectional FG structures, the developed HSDT model can be implemented.

Table 4 Non-dimensional fundamental frequency parameters of porous FG square plate

Support Condition	n_z	Sharma *et al.* (2021)	Present HSDT	% Difference
SSSS	0	6.4971	6.2658	3.5600
	0.3	5.6564	5.4607	3.4598
	0.5	5.1681	5.0278	2.7147
	1	4.2822	4.2041	1.8238
	2	3.5332	3.5025	0.8689
CCCC	0	11.8128	11.7122	0.8516
	0.3	10.3914	10.3012	0.8680
	0.5	9.4503	9.3725	0.8233
	1	7.9737	7.9139	0.7500
	2	6.4883	6.4463	0.6473

Table 5 Non-dimensional fundamental frequency parameters of unidirectional FG plate

Approach	n_z					
	0	0.5	1	5	10	100
Present HSDT	5.7697	4.0256	3.5415	2.8890	2.7507	2.5701
ANSYS-APDL	5.7417	3.9721	3.4810	2.8396	2.7057	2.5236

Table 4 shows a comparison of findings from the current finite element formulation with those from the literature (Sharma *et al.* 2021). In this illustration, the nondimensional fundamental frequency parameters of a porous square 1D-FGM plates with *SSSS* and *CCCC* support conditions, power law exponents (n_z = 0 to 2) and thickness ratio h/a = 0.02 is carried out. The even type of porosity is considered with porosity index 0.2 for all the cases. The plates are comprised of Aluminium (Al) and Alumina (Al_2O_3). The dimension less fundamental frequency values are computed and compared to the findings of Sharma *et al.*, (2021). The data indicate that, the percentage difference between the present results and the results of Sharma *et al.*, (2021) is less than 4%. Hence, the current findings demonstrate a strong agreement with the existing literature.

Further to show the accuracy of the proposed HSDT model, the nondimensional fundamental frequency parameters of unidirectional FG plates with SUS304 and Si_3N_4, a/b = 1 and a/h = 10 are compared with the results obtained through the ANSYS-APDL platform, which are depicted in the Table 5. The results of proposed HSDT model shows excellent agreement with the results obtained through the ANSYS software package, which confirms the accuracy of present model.

3.2 Study of perfect-imperfect (without and with porosity) FGM

In this part, the free vibrational behavior of bidirectional and multidirectional perfect-imperfect FGM structure is examined against various power law index, boundary conditions, aspect and thickness ratio, and for curvature of shell geometry. Also, non-dimensional fundamental frequency evaluated as, $\bar{\omega} = \omega(a^2/h)\sqrt{(\rho/E)_c}$.

3.2.1 Perfect and Imperfect 2D FGM structure

The Power-law index is important for designing bi-directional FG structures because it specifies the volume fraction of metal and ceramic in the FG structures, which in turn influences the structure's stiffness. Table 6 shows the nature of fundamental frequency variation with the variation in power law index. During the study FGM plate with three different combinations of Power-law indices, aspect ratio 1.5, thickness ratio 50, under all side clamped boundary conditions is considered. It is observed that, NFF is maximum for n_x variation, but as soon as power law index varied beyond 1 the NFF became maximum for the n_z variation. It is also observed that, maximum NFF is observed in perfect FGM structure than porous structures. The percentage deviations in case of uneven porosity distribution as compared to perfect FGM structure is 1.46, 1.52, 1.59 and 1.66 respectively. Similarly, the percentage deviation in the case of even porosity distribution as compared to perfect FGM structure is 5.61, 5.86, 6.16 and 6.44 respectively. It is also worth noting that as the Power-law index value rises, the NFF value falls in all three cases. This is because as the power-law index value increases, the FGM structures become more metal-rich, and Stainless Steel has a lower stiffness than Silicon Nitride.

The influence of thickness ratio (10, 20, 50, 100) on NFF of 2D porous FG completely clamped plates with a/b = 1.5 and three separate Power-law index pairings is shown in Table 7. There are some important observations are noted from the analysis. The porosity in 2D-FG plates causes a decrease in NFF value. The percentage decrement in NFF for even porosity distribution for porosity indices 0.1, 0.2 0.3 are 6.26, 13.90, 23.48 respectively, and for uneven porosity distribution are 2.06, 4.33, 6.84 respectively. If the findings of example-1 (Power law indices n_x = 1 and n_y = 1) and example-2 (Power law indices n_y = 1 and n_z = 1) are compared, then the percentage difference in NFF is 0.36, 0.37, 0.38, 0.39 for without and with porosity considering porosity index 0.1, 0.2, 0.3 respectively, similarly that difference is 0.36, 0.38, and 0.39 for uneven type of

Table 6 Effect of Power-law index on NFF of bidirectional FG plates

Power-law Index			Porosity type and index						
			No Porosity	Even Porosity			Uneven Porosity		
n_x	n_y	n_z	0	0.1	0.2	0.3	0.1	0.2	0.3
0.5	1	0	10.5143	9.924	9.2953	8.6193	10.3606	10.2038	10.0434
1			9.8407	9.2636	8.6471	7.9820	9.6907	9.5375	9.3806
2			9.1717	8.6068	8.0014	7.3454	9.0252	8.8753	8.7218
5			8.6243	8.0685	7.4712	6.8214	8.4804	8.3331	8.1820
0	0.5	1	10.5141	9.9193	9.2849	8.6011	10.3585	10.1995	10.0367
	1		9.8562	9.2765	8.6567	7.9868	9.7050	9.5504	9.3921
	2		9.2229	8.6588	8.0543	7.3990	9.0763	8.9263	8.7726
	5		8.6965	8.1445	7.5518	6.9076	8.5534	8.4071	8.2570
1	0	0.5	10.3533	9.7628	9.1333	8.4554	10.1996	10.0427	9.8823
		1	9.8434	9.2644	8.6456	7.9769	9.6925	9.5382	9.3802
		2	9.4051	8.8386	8.2319	7.5746	9.2571	9.1057	8.9504
		5	8.9939	8.4395	7.8453	7.2008	8.8491	8.7009	8.5487

Table 7 Influence of thickness ratio on NFF of bidirectional FG plates

Power-law Index			*a/h*	Porosity type and index						
				No Porosity	Even Porosity			Uneven Porosity		
n_x	n_y	n_z		0	0.1	0.2	0.3	0.1	0.2	0.3
1	1	0	10	7.9787	7.508	7.0049	6.4615	7.8169	7.6472	7.4677
			20	9.1188	8.5826	8.0098	7.3914	8.9653	8.807	8.6429
			50	9.8407	9.2636	8.6471	7.982	9.6907	9.5375	9.3806
			100	10.0535	9.4643	8.8350	8.1561	9.9063	9.7566	9.6040
0	1	1	10	8.0075	7.5360	7.0319	6.4870	7.8458	7.6764	7.4974
			20	9.1407	8.6027	8.0276	7.4059	8.9866	8.8276	8.6629
			50	9.8562	9.2765	8.6567	7.9868	9.7050	9.5504	9.3921
			100	10.067	9.4749	8.8419	8.1578	9.9184	9.7670	9.6127
1	0	1	10	7.9919	7.5211	7.0177	6.4739	7.4833	7.6617	7.4833
			20	9.1264	8.5891	8.0148	7.3942	8.6495	8.8138	8.6495
			50	9.8434	9.2644	8.6456	7.9769	9.3802	9.5382	9.3802
			100	10.0541	9.4628	8.8307	8.1478	9.6008	9.7548	9.6008

porosity distribution. If the findings of example-2 (Power law indices $n_y = 1$ and $n_z = 1$) and example-3 (Power law indices $n_x = 1$ and $n_z = 1$) are compared, then percentage difference in NFF is 0.195, 0.198, 0.202, and 0.202 for without and with porosity considering porosity index 0.1, 0.2, 0.3 respectively, similarly that difference is 4.84, 0.191, and 0.188 for uneven type of porosity distribution. During the study, the density of the FGM plate maintained constant, which means that the stiffness of the plate was reduced due to induced porosity in the plate.

The influence of four distinct aspect ratio on NFF of 2D-FG fully clamped plates with $a/h = 50$ and three distinct Power-law index pairings is demonstrated though the Figs. 5(a) to 5(c). The NFF is computed for 2D-FG plates without and with porosity (even and uneven), the percentage of porosity also varied to observe the effect on NFF. The outcome demonstrates that as aspect ratio (a/b) increases, non-dimensional fundamental frequency increases. Also, as the porosity index value increases, the overall stiffness of the 2D-FG plate structure drops, resulting in a decrease in NFF value. Additionally, with higher porosity index values, the even type of porosity distribution pattern exhibits diminished strength in comparison to the uneven distribution pattern.

The support conditions are practically necessary for problem definition and have utmost significance in structural analysis. This is due to the fact that how things are numerically treated may have a substantial impact on the applicability of numerical methods and the quality of computations that occur. The support conditions are essential while utilizing FEA to address computation problems. The proper realistic support conditions must be applied to utilize FEA to its fullest extent. In this section, the effect of distinct support conditions on the free vibrational behavior of bidirectional FG plates is discussed. The NFF of bi-directional porous FG plates with material properties gradation in three different pairs of directions ($n_x = n_y = 1$, $n_y = n_z = 1$ and $n_z = n_x = 1$) for different support conditions are listed in Table 8. The aspect ratio and thickness ratio of the plate are kept at 1.5 and 50, respectively for all the cases. It is noticed that, because of the number of degrees of freedom, the maximum NFF value is recorded for the 2D-FG plate with CCCC support condition, while the lowest is recorded for the CFFF support condition in all instances. The NFF value increases, as the number of degrees of freedom of the FG structures restrict. The maximum NFF value is recorded in perfect FGM plates compared to porous FGM plates and it is

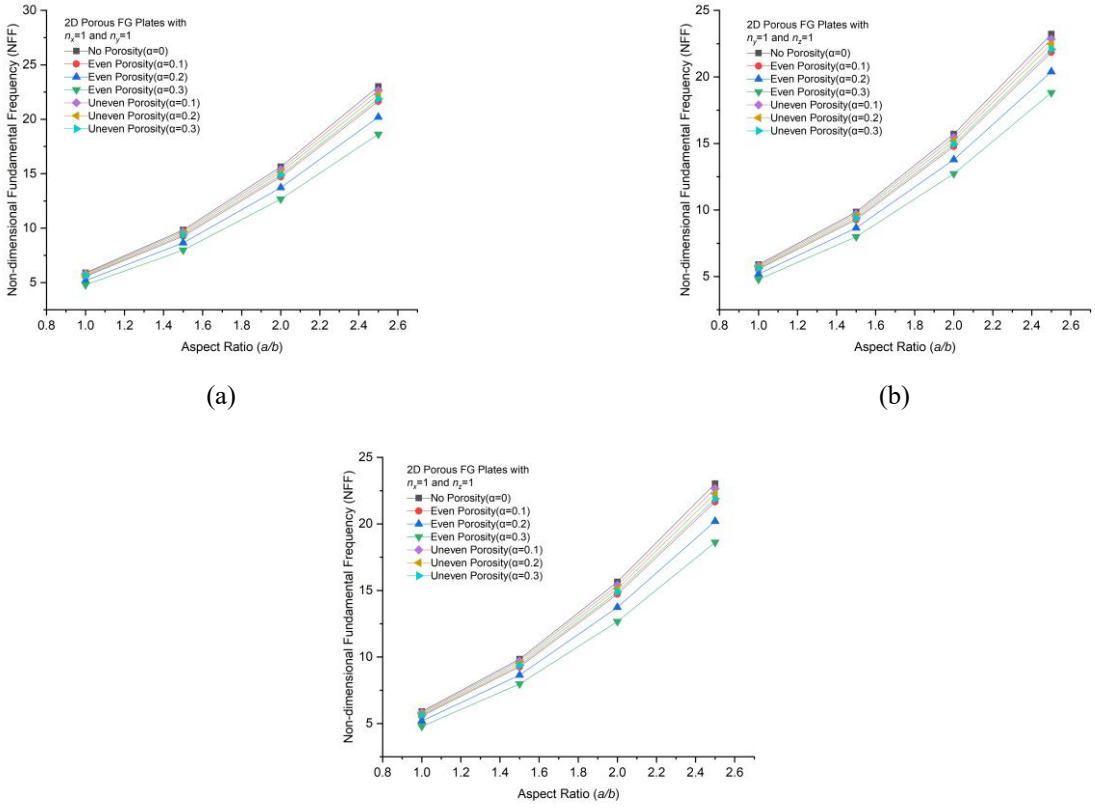

Fig. 5 Effect of aspect ratio on NFF in case of bidirectional FGM

Table 8 Effect of support condition on NFF in case of bidirectional FGM

Power-law Index			Support Condition	Porosity type and index						
				No Porosity	Even Porosity			Uneven Porosity		
n_x	n_y	n_z		0	0.1	0.2	0.3	0.1	0.2	0.3
1	1	0	CCCC	9.8407	9.2636	8.6471	7.982	9.6907	9.5375	9.3806
			SCSC	9.0010	8.4692	7.9007	7.2866	8.8632	8.7226	8.5786
			SSSS	4.9264	4.6364	4.3277	3.9945	4.8541	4.7816	4.7078
			CFFF	1.9213	1.8063	1.6833	1.5504	1.8925	1.8632	1.8333
0	1	1	CCCC	9.8562	9.2765	8.6567	7.9868	9.7050	9.5504	9.3921
			SCSC	9.0594	8.5263	7.9564	7.3403	8.9207	8.7788	8.6336
			SSSS	4.9345	4.6445	4.3344	3.9994	4.8626	4.7894	4.7148
			CFFF	1.8115	1.7053	1.5917	1.4689	1.7848	1.7576	1.7299
1	0	1	CCCC	9.8434	9.2644	8.6456	7.9769	9.6925	9.5382	9.3802
			SCSC	9.0031	8.4698	7.8995	7.2826	8.8646	8.7231	8.5782
			SSSS	4.9251	4.6349	4.3246	3.9892	4.8532	4.7799	4.7054
			CFFF	1.8775	1.7647	1.6439	1.5133	1.8492	1.8203	1.7909

maximum for FGM plates with uneven kind of porosity than even porosity, as expected.

Table 9 shows the free vibrational responses of bi-directional fully clamped porous FG curved structures such as spherical, cylindrical, elliptical, and hyperboloid at two different curvature ratios (R/a = 10 and 50). To observe the effect of curvature ratio and geometry shapes along with porosity type, the NFF of 2D-FG curved structure without and with porosity are computed for different pairs of Power-law indices. The aspect ratio and thickness ratio of the curved structures are kept at 1.5 and 50, respectively for all the cases. It is noticed that, the NFF value drops as the curvature ratio increases like 1D-FG structures. The highest NFF is recorded for the 2D FG perfect spherical structure. The NFF value drops with an increase in porosity percentage in the curved structures. The influence of geometrical shapes of curved structures on the NFF value is minor, while the effect of curvature ratio and porosity type is substantial.

Table 9 Effect of curvature of shell geometry on NFF in case of bidirectional FGM

R/a	Power-law Index			Curved Structure	Porosity type and index						
					No Porosity	Even Porosity			Uneven Porosity		
	n_x	n_y	n_z		0	0.1	0.2	0.3	0.1	0.2	0.3
10	1	1	0	Spherical	10.4361	9.8234	9.169	8.4626	10.2613	10.0826	9.8997
				Cylindrical	10.0913	9.4992	8.8668	8.1844	9.9307	9.7667	9.5988
				Elliptical	10.2077	9.6086	8.9688	8.2782	10.0423	9.8732	9.7002
				Hyperbolic	10.207	9.6081	8.9685	8.2782	10.0417	9.8727	9.6998
	0	1	1	Spherical	10.4633	9.8494	9.1934	8.4848	10.2876	10.1080	9.924
				Cylindrical	10.1111	9.5169	8.8818	8.1956	9.9494	9.7842	9.6149
				Elliptical	10.2305	9.6298	8.9877	8.2941	10.0641	9.8940	9.7198
				Hyperbolic	10.2251	9.6236	8.9805	8.2853	10.0585	9.8881	9.7135
	1	0	1	Spherical	10.4441	9.8305	9.1748	8.4666	10.2687	10.0893	9.9056
				Cylindrical	10.0966	9.5032	8.869	8.1839	9.9353	9.7704	9.6016
				Elliptical	10.2139	9.6137	8.9722	8.2793	10.0478	9.8780	9.7041
				Hyperbolic	10.2133	9.6131	8.9717	8.2788	10.0473	9.8775	9.7036
50	1	1	0	Spherical	9.8653	9.2866	8.6686	8.0018	9.7142	9.5599	9.402
				Cylindrical	9.8509	9.2731	8.656	7.9902	9.7004	9.5467	9.3894
				Elliptical	9.8557	9.2776	8.6602	7.994	9.705	9.5511	9.3936
				Hyperbolic	9.8557	9.2776	8.6602	7.994	9.705	9.5511	9.3936
	0	1	1	Spherical	9.8818	9.3008	8.6797	8.0085	9.7296	9.5740	9.4147
				Cylindrical	9.8666	9.2864	8.666	7.9955	9.7150	9.5600	9.4012
				Elliptical	9.8718	9.2913	8.6707	8.0000	9.7200	9.5648	9.4058
				Hyperbolic	9.8709	9.2902	8.6694	7.9983	9.7190	9.5637	9.4047
	1	0	1	Spherical	9.8683	9.288	8.6677	7.9975	9.7296	9.5740	9.4147
				Cylindrical	9.8538	9.2744	8.6549	7.9857	9.7150	9.5600	9.4012
				Elliptical	9.8587	9.2789	8.6592	7.9896	9.7200	9.5648	9.4058
				Hyperbolic	9.8587	9.2789	8.6592	7.9896	9.7190	9.5637	9.4047

3.2.2 Perfect and Imperfect 3D FGM structure

In section 3.2.1, it was observed the performance of the FGM plate whose material property gets varied in any two directions. But the new kind of analysis is presented in section 3.2.2, in which FGM plate is presented whose material properties are varied in all three directions. During the evaluation of NFF, various parameters are varied, like plate aspect ratio and thickness ratio, boundary conditions, nature of the shell panel.

The material properties of multi-directional FG plates are graded in three distinct directions, which is accomplished by n_x, n_y and n_z Power-law indices. It is well known that any structure's stiffness affects its capacity to react vibrations, and the stiffness of a FGM structure is linked to the volume fraction of the FGM elements (Metal and Ceramic). The volume fraction of FGM elements controlled by Power-law indices. Hence, the influence of Power-law index on free vibrational behavior of multi-directional FG plates are studied in this section. Table 10 shows the NFF of multi-directional FG plates without and with porosity for various power law indices in *x*, *y,* and *z* direction variation. During the analysis plate thickness ratio and aspect ratio are maintained at 50 and 1.5 respectively under all side clamped condition. To analyze the effect each power-law index n_x, n_y, and n_z, one power law exponent gets varied and the other two are maintained constant. A higher Power-law exponent value results in a lower ceramic volume percentage in the FGM, which results in a lower overall stiffness and lower corresponding fundamental frequency values. As a result, the findings of the analysis demonstrate a striking fall in frequency values with an increase in power exponent values. Additionally, depending on the values of the Power-law exponents and porosity index, the non-dimensional frequencies of multi-directional porous FG plates can be controlled.

The NFF of 3D-FG plates without and with porosity, considering a/b = 1.5, two different Power-law indices (n_x = n_y = n_z = 1 and 5) and four distinct thickness ratios (a/h = 10, 20, 50 and 100) are plotted, which are depicted in the Figs. 6 and 7. The stiffness value of any structure drops with a reduction of its thickness which results drop in frequency. Hence, the NFF value drops with a decrease in thickness ratio. The NFF value is higher for perfect 3D-FG plates compared to porous 3D-FG plates. Also, it is worth noting that, with higher porosity index values, the even kind of porosity distribution has less strength than the uneven distribution pattern.

Table 11 shows the NFF of 3D-FG plates without and with porosity, considering a/h = 50, different Power-law indices (n_x = n_y = n_z = 1, 2 and 5) and four distinct aspect ratios (a/b = 10, 20, 50 and 100). It is noticed that, as the aspect ratio rises, the non-dimensional fundamental frequency values increase in all cases, this is due to the relation of length and the stiffness. As the porosity index value rises, the overall stiffness of 3D-FGM structures decreases, which results fall in frequency values. Additionally, with higher porosity index values, the even kind of porous demographic factor exhibits diminished strength compared to the uneven distribution pattern.

Table 10 Effect of Power law index on NFF in case of multi-directional FGM plate

Power-law Index			Porosity type and index						
			No Porosity	Even Porosity			Uneven Porosity		
n_x	n_y	n_z	0	0.1	0.2	0.3	0.1	0.2	0.3
0.5	1	1	9.3879	8.8178	8.2075	7.5466	9.2396	9.088	8.9326
1			9.1020	8.5372	7.9317	7.275	8.9553	8.8053	8.6515
2			8.7961	8.2365	7.6357	6.9828	8.6510	8.5025	8.3503
5			8.5267	7.9711	7.3736	6.7231	8.3828	8.2355	8.0845
1	0.5	1	9.3738	8.8034	8.1927	7.5315	9.2255	9.0738	8.9184
	1		9.1020	8.5372	7.9317	7.275	8.9553	8.8053	8.6515
	2		8.8191	8.2607	7.6613	7.0102	8.6742	8.5261	8.3742
	5		8.5639	8.0106	7.416	6.769	8.4206	8.2739	8.1236
1	1	0.5	9.3231	8.7538	8.1443	7.4844	9.1753	9.0243	8.8696
		1	9.1020	8.5372	7.9317	7.2750	8.9553	8.8053	8.6515
		2	8.9043	8.3448	7.7445	7.0926	8.7588	8.6100	8.4574
		5	8.7089	8.1546	7.5594	6.9127	8.5647	8.4172	8.2658

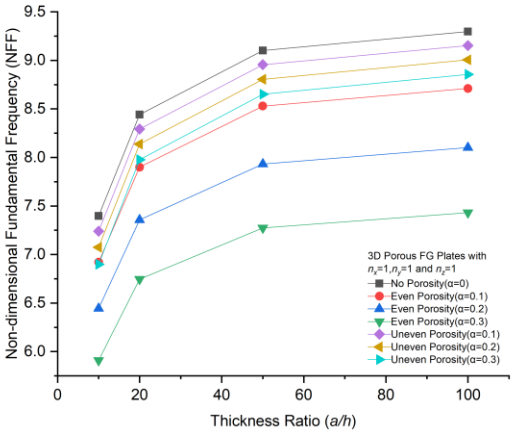

Fig. 6 Influence of thickness ratio on NFF of 3D porous FG plates with $n_x = n_y = n_z = 1$

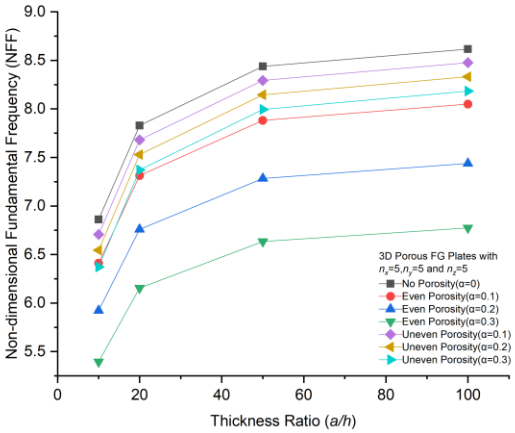

Fig. 7 Influence of thickness ratio on NFF of 3D porous FG plates with $n_x = n_y = n_z = 5$

The non-dimensional fundamental frequency responses of the 3D-FG ($SUS304/Si_3N_4$) plates with a/h = 50, a/b = 1.5 are computed considering the perfect and porous form of the plate, which are presented in the Table 12. Four types of boundary conditions are utilized in the study, SSSS: all sides simply supported, CCCC: all sides are rigidly

Table 11 Influence of aspect ratio on NFF of 3D porous FG plates

Power-law Index			a/b	Porosity type and index						
				No Porosity	Even Porosity			Uneven Porosity		
n_x	n_y	n_z		0	0.1	0.2	0.3	0.1	0.2	0.3
1	1	1	1	5.4546	5.1163	4.7536	4.3603	5.3685	5.2807	5.1909
			1.5	9.1020	8.5372	7.9317	7.275	8.9553	8.8053	8.6515
			2	14.4915	13.5913	12.6262	11.5793	14.2525	14.0077	13.7562
			2.5	21.4115	20.0793	18.6508	17.1011	21.0512	20.6814	20.3005
2	2	2	1	5.1439	4.8112	4.4537	4.0646	5.0595	4.9732	4.885
			1.5	8.5856	8.0302	7.4333	6.7838	8.4416	8.2943	8.1431
			2	13.6771	12.7921	11.8409	10.8058	13.4425	13.202	12.9547
			2.5	20.2261	18.9168	17.5094	15.9778	19.8725	19.5092	19.1347
5	5	5	1	5.0548	4.7222	4.3642	3.9742	4.9705	4.8843	4.7961
			1.5	8.4371	7.8819	7.2844	6.6333	8.2933	8.1461	7.9951
			2	13.442	12.5573	11.6053	10.5679	13.2077	12.9675	12.7204
			2.5	19.8819	18.5733	17.1652	15.6308	19.5289	19.1661	18.7919

Table 12 Influence of support condition on NFF of 3D porous FG plates

Power-law Index			Support Condition	Porosity type and index						
				No Porosity	Even Porosity			Uneven Porosity		
n_x	n_y	n_z		0	0.1	0.2	0.3	0.1	0.2	0.3
1	1	1	CCCC	9.1020	8.5372	7.9317	7.2750	8.9553	8.8053	8.6515
			SCSC	8.3564	7.8368	7.2796	6.6752	8.2218	8.0841	7.9431
			SSSS	4.5556	4.2729	3.9697	3.6409	4.4858	4.4148	4.3424
			CFFF	1.6969	1.5905	1.4763	1.3523	1.6703	1.6432	1.6155
2	2	2	CCCC	8.5856	8.0302	7.4333	6.7838	8.4416	8.2943	8.1431
			SCSC	7.8963	7.3857	6.8368	6.2395	7.7642	7.6290	7.4904
			SSSS	4.3020	4.0238	3.7248	3.3994	4.2334	4.1637	4.0926
			CFFF	1.5910	1.4876	1.3765	1.2554	1.5652	1.5389	1.5121
5	5	5	CCCC	8.4371	7.8819	7.2844	6.6333	8.2933	8.1461	7.9951
			SCSC	7.7581	7.2478	6.6987	6.1004	7.6262	7.4912	7.3527
			SSSS	4.2262	3.9483	3.6494	3.3237	4.1578	4.0881	4.0172
			CFFF	1.5445	1.4428	1.3334	1.2141	1.5191	1.4933	1.4669

clamped, SCSC: alternate simply supported and clamping of the plate edges, and CFFF: one edge is clamped and remaining sides are free which can be termed as cantilever plate condition. It is noticed that the maximum number of constraints are provided in CCCC boundary condition more than any other, so the FGM plate became stiff and maximum NFF associated with it, while lowest with CFFF, because of the cantilever boundary condition. Also, it is interesting to note that the free vibration results gradually decrease in value as follows: CCCC > SCSC > SSSS > CFFF.

Table 13 shows the effect of various multi-directional porous FG curved structures on dimensionless fundamental frequency for different power law index. The curved structures considered for this study are perfect (without porosity) and imperfect (even and uneven porosity) in nature and tabulated result to find the distinguishing performance. The percentage increment in panel stiffness and hence fundamental frequency as we shift from Cylindrical to Elliptical, Elliptical to Hyperbolic, Hyperbolic to Spherical which is 1.15, 0.022, and 2.26 respectively.

Further, whenever the shift from perfect to the porous structure, the NFF is reduced and the average decrement is 15.5 and 4.9 percent respectively for even and uneven distribution. Next, when comparing the NFF for $n_x = n_y = n_z = 1$ and 2, then observation shows that NFF is get reduced by 6.07, 6.08, 6.032, 6.14 for Cylindrical, Elliptical, Hyperboloid, and Spherical structures respectively and similarly that difference is 7.904, 7.892, 7.902, 7.93 percent for $n_x = n_y = n_z = 2$ and 5. Moreover, the NFF value decreases with an increase in curvature ratio.

3.2.3 Comparative Analysis of unidirectional (1D) and multidirectional (2D and 3D) FGMs

In this section, the comparative study of free vibration responses of unidirectional and multidirectional FGMs is provided by keeping the same geometrical parameters. Fig. 8 shows the non-dimensional frequency parameters of the perfect FG plates. It is observed that the, NFP shows the lower values for bidirectional FGM plates compare to unidirectional FGM and it is again decreases for the multidirectional FGM plates. Fig. 9 depicts the non-dimensional fundamental frequency parameters of unidirectional, bidirectional, and multidirectional porous FGM plates for different even porosity index. It is observed that the NFF values shows the declining trend with an increasing porosity index. For all cases, the NFF value

Table 13 Influence of curvature ratio and geometry shape on NFF of 3D porous FG curved structures

R/a	Power-law Index			Curved Structure	Porosity type and index						
					No Porosity	Even Porosity			Uneven Porosity		
	n_x	n_y	n_z		0	0.1	0.2	0.3	0.1	0.2	0.3
10	1	1	1	Cylindrical	9.3363	8.7571	8.1363	7.4632	8.8542	9.0188	8.8542
				Elliptical	9.4432	8.8572	8.229	7.5478	8.9464	9.116	8.9464
				Hyperbolic	9.4453	8.8596	8.2317	7.5509	8.9488	9.1183	8.9488
				Spherical	9.6589	9.0601	8.4182	7.7223	9.1342	9.3134	9.1342
	2	2	2	Cylindrical	8.8020	8.2321	7.6196	6.9531	8.6478	8.49	8.328
				Elliptical	8.9020	8.3254	7.7056	7.0312	8.7432	8.5805	8.4136
				Hyperbolic	8.9080	8.3313	7.712	7.0381	8.7487	8.5862	8.4194
				Spherical	9.1006	8.5108	7.8768	7.1869	8.9326	8.7606	8.584
	5	5	5	Cylindrical	8.6524	8.0827	7.4698	6.8018	8.4984	8.3407	8.1788
				Elliptical	8.7524	8.176	7.5559	6.88	8.5937	8.4312	8.2644
				Hyperbolic	8.7536	8.1775	7.5576	6.882	8.5949	8.4325	8.2658
				Spherical	8.9493	8.3599	7.7257	7.0345	8.7816	8.6097	8.4333
50	1	1	1	Cylindrical	9.1116	8.5462	7.9401	7.2829	8.9645	8.814	8.6598
				Elliptical	9.1159	8.5502	7.9437	7.286	8.9685	8.8179	8.6634
				Hyperbolic	9.1162	8.5505	7.9442	7.2866	8.9688	8.8182	8.6638
				Spherical	9.1252	8.559	7.9521	7.2939	8.9775	8.8264	8.6716
	2	2	2	Cylindrical	8.5938	8.0379	7.4403	6.79	8.4494	8.3017	8.1501
				Elliptical	8.5976	8.0413	7.4434	6.7928	8.453	8.305	8.1532
				Hyperbolic	8.5989	8.0427	7.4449	6.7944	8.4543	8.3064	8.1546
				Spherical	8.6055	8.0487	7.4502	6.7989	8.4605	8.3121	8.1599
	5	5	5	Cylindrical	8.4457	7.8898	7.2917	6.6399	8.3014	8.1538	8.0023
				Elliptical	8.4497	7.8935	7.2951	6.6429	8.3052	8.1574	8.0057
				Hyperbolic	8.4501	7.894	7.2956	6.6435	8.3057	8.1578	8.0061
				Spherical	8.4578	7.9011	7.302	6.6492	8.313	8.1647	8.0126

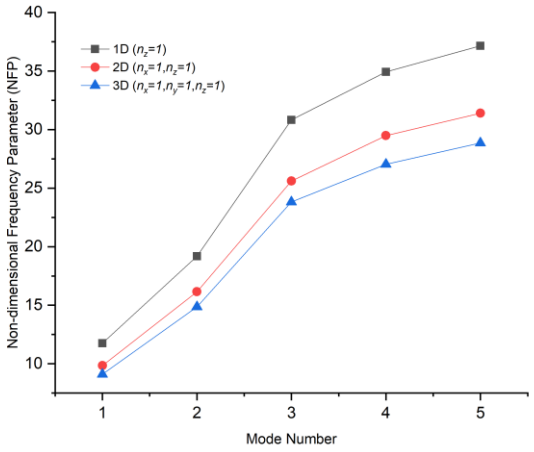

Fig. 8 NFP of unidirectional and multidirectional perfect FG plates

reduces as the material is graded from one direction to two directions, and it lowers again when the gradation is altered from two directions to three directions.

4. Conclusions

The free vibrational behavior of bi-directional and multi-directional porous FG plates and curved structures (spherical, cylindrical, elliptical, and hyperboloid) are provided using HSDT based 2D-FEM model in the current study. The non-dimensional fundamental frequencies of FGM plates and curved structures without and with porosity (even and uneven) are computed. The FG graded structures are comprised of Stainless Steel (*SUS304*) and Silicon Nitride (Si_3N_4) material. The heterogeneous material properties of the porous FGMs are estimated using Voigt's Model of material distribution via Power-law function. The higher order 2D-FEM formulation is implemented on a computer by writing the necessary computer code in the

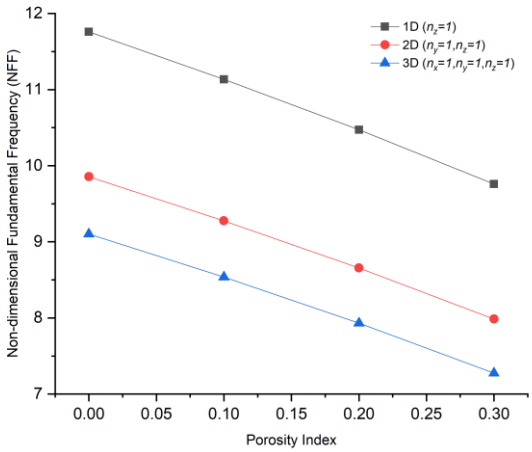

Fig. 9 NFF of unidirectional and multidirectional porous FG plates

MATLAB environment. To ensure the accuracy and efficacy of the developed 2D-FEM model, the convergence and validation study is presented. Further, the research is extended and an inclusive parametric analysis is carried out to investigate the developed model through some new numerical experiments to test the robustness of the developed model. The influence of Power-law indices, thickness and aspect ratios, support condition, porosity type and porosity index on dimensionless fundamental frequencies of unidirectional, bi-directional, and multi-directional porous FG plates and curved structures has been discussed through different numerical examples. Based on the obtained results, the following concluding remarks are listed;

- The proposed HSTD model is well converged to an element size of 5×5, revealing that this mesh size is adequate for computing free vibration responses of perfect and porous FG plates and curved structures.
- The results of the proposed HSDT model accord well with those that have been reported in the literature, which indicate the efficacy and the suitability of the developed model to predict the free vibrational responses of multidirectional FG plate and curved structures with and without porosity.
- The free vibration of multidirectional FG plates and curved structures with and without porosity is greatly influenced by the material attributes, geometrical attributes, support conditions, percentage of porosity, and type of porosity.
- A Power-law exponent value decides the volume fraction of FGM constituents, a greater Power-law exponent value in bi-directional and multidirectional FG plates and curved structures leads in a smaller ceramic volume percentage, which results in a lower overall stiffness and lower corresponding fundamental frequency values. As a result, the investigation's findings demonstrate a considerable fall in frequency values as power exponent values rise.
- The free vibrational responses of any structure are greatly influenced by its thickness, the stiffness value of any structure falls as its thickness decreases, resulting in a drop in frequency. This study reveals that the dimensionless frequency value drops as the thickness ratio lowers in bi-directional and multi-directional FG plates with and without porosity.
- The dimensionless frequency value of bidirectional and multidirectional FG plates with and without porosity significantly increases when aspect ratio rises from lower to higher values. The non-dimensional fundamental frequency value increased by more than 30% when the geometry changed from square shape (a/b = 1) to rectangular shape (a/b = 1.5).
- The kind of support conditions has a significant impact on the natural frequency of the FGM structures. The maximum number of constraints are provided in CCCC boundary condition than any other, so the bi-directional and multi-directional FGM plates with and without porosity became stiff and maximum NFF associated with it, while lowest with CFFF, because of the cantilever boundary condition and the free vibration results gradually decrease in value as follows: CCCC > SCSC > SSSS > CFFF.
- The dimensionless fundamental frequency value shows a decreasing trend with an increment of curvature ratio. The spherical structure is the stiffest of the geometries offered, while the cylindrical surface is the most flexible. Also, it is worth to note that the influence of geometrical shapes of curved structures on the NFF value is minor, while the effect of curvature ratio and porosity type is substantial.
- The dimension less frequency value reduces as the material is graded from one direction to two directions, and it lowers again when the gradation is altered from two directions to three directions. Hence, the natural frequency value decreases when the unidirectional FGMs are replaced with multidirectional FGMs for the same structures.
- The perfect FGM plates and curved structures have the highest NFF values compared to porous FGM

plates and curved structures, also it is maximum for FGM plates and curved structures with uneven kind of porosity than even porosity for constant geometrical parameters and the Power-law indices.

- This developed generalized HSDT computational model will be the reference for the designers and researchers to predict the free vibration behaviour of multi-directional FGMs for better design and continuation of research in this area. Moreover, this study helps designer to design structures that are lighter and more durable for a variety of engineering applications specially in the aerospace and automobile sector.

References

Ahlawat, N. and Lal, R. (2016), "Buckling and vibrations of multi-directional functionally graded circular plate resting on elastic foundation", *Proc. Eng.*, **144**, 85-93. https://doi.org/10.1016/j.proeng.2016.05.010.

Al Rjoub, Y.S. and Alshatnawi, J.A. (2020), "Free vibration of functionally-graded porous cracked plates", *In Struct.*, **28**, 2392-2403. https://doi.org/10.1016/j.istruc.2020.10.059.

Bansal, G., Gupta, A. and Katiyar, V. (2020), "Vibration of porous functionally graded plates with geometric discontinuities and partial supports", *Proc. of the Instit. of Mech. Enginrs., Part C: J. of Mech. Engg. Sci.*, **234**(21), 4149-4170. https://doi.org/10.1177/0954406220920660.

Bathini, S.R. (2020), "Free vibration behavior of bi-directional functionally graded plates with porosities using a refined first order shear deformation theory", *J. Comput. Appl. Mech.*, **51**(2), 374-388. https://doi.org/10.22059/JCAMECH.2020.303046.510.

Chen, M., Jin, G., Ma, X., Zhang, Y., Ye, T. and Liu, Z. (2018), "Vibration analysis for sector cylindrical shells with bi-directional functionally graded materials and elastically restrained edges", *Compos. Part B: Eng.*, **153**, 346-363. https://doi.org/10.1016/j.compositesb.2018.08.129.

Cuong-Le, T., Nguyen, K.D., Lee, J., Rabczuk, T. and Nguyen-Xuan, H. (2021), "A 3D nano scale IGA for free vibration and buckling analyses of multi-directional FGM nanoshells", *Nanotech.*, **33**(6), 065703. https://doi.org/10.1088/1361-6528/ac32f9.

Ebrahimi, M.J. and Najafizadeh, M.M. (2014), "Free vibration analysis of two-dimensional functionally graded cylindrical shells", *Appl. Math. Model.*, **38**(1), 308-324. https://doi.org/10.1016/j.apm.2013.06.015.

Esmaeilzadeh, M. and Kadkhodayan, M. (2019), "Dynamic analysis of stiffened bi-directional functionally graded plates with porosities under a moving load by dynamic relaxation method with kinetic damping", *Aerosp. Sci. Tech.*, **93**,105333. https://doi.org/10.1016/j.ast.2019.105333.

Ghatage, P.S., Kar, V.R. and Sudhagar, P.E. (2020), "On the numerical modelling and analysis of multi-directional functionally graded composite structures: A review", *Compos. Struct.*, **236**, 111837. https://doi.org/10.1016/j.compstruct.2019.111837.

Ghatage, P.S. and Sudhagar, P.E. (2023), "Free vibrational behavior of bi-Directional functionally graded composite panel with and without porosities using 3D finite element approximations", *Int. J. Integra. Eng.*, **15**(1), 131-144. https://doi.org/10.30880/ijie.2023.15.01.012.

Ghatage, P.S. and Sudhagar, P.E. (2023), "Free vibrational behavior of bi-directional perfect and imperfect axially graded cylindrical shell panel under thermal environment", *Struct. Eng. Mecha.*, **85**(1), 135. https://doi.org/10.12989/sem.2023.85.1.135..

Hadji, L., Bernard, F., Safa, A. and Tounsi, A. (2021), "Bending and free vibration analysis for FGM plates containing various distribution shape of porosity", *Adv. Mater. Res.*, **10**(2), 115-135. https://doi.org/10.12989/amr.2021.10.2.115.

Hosseini-Hashemi, S., Salehipour, H., Atashipour, S.R. and Sburlati, R. (2013), "On the exact in-plane and out-of-plane free vibration analysis of thick functionally graded rectangular plates: Explicit 3-D elasticity solutions", *Compos. Part B: Eng.*, **46**, 108-115. https://doi.org/10.1016/j.compositesb.2012.10.008.

Kang, R., Xin, F., Shen, C. and Lu, T.J. (2022), "3D free vibration analysis of functionally graded plates with arbitrary boundary conditions in thermal environment", *Adv. Eng. Materi.*, **24**(5), 2100636. https://doi.org/10.1002/adem.202100636.

Kar, V.R. and Panda, S.K. (2015a), "Free vibration responses of temperature dependent functionally graded curved panels under thermal environment", *Latin Am. J. Sol. Struct.*, **12**(11), 2006-2024. https://doi.org/10.1590/1679-78251691.

Kar, V.R. and Panda, S.K. (2015b), "Thermoelastic analysis of functionally graded doubly curved shell panels using nonlinear finite element method", *Compos. Struct.*, **129**, 202-212. https://doi.org/10.1016/j.compstruct.2015.04.006.

Kar, V.R. and Panda, S.K. (2016), "Nonlinear thermomechanical deformation behaviour of P-FGM shallow spherical shell panel", *Chine. J. Aeron.*, **29**(1), 173-183.

Keddouri, A., Hadji, L. and Tounsi, A. (2019), "Static analysis of functionally graded sandwich plates with porosities", *Adv. Mater. Res.*, **8**(3), 155-177. https://doi.org/10.12989/amr.2019.8.3.155.

Khiloun, M., Bousahla, A.A., Kaci, A., Bessaim, A., Tounsi, A. and Mahmoud, S.R. (2020), "Analytical modeling of bending and vibration of thick advanced composite plates using a four-variable quasi 3D HSDT", *Eng. with Comput.*, **36**(3), 807-821. https://doi.org/10.1007/s00366-019-00732-1.

Li, S., Zheng, S. and Chen, D> (2020), "Porosity dependent isogeometric analysis of bi-directional functionally graded plates", *Thin-Walled Struct.*, **156**, 106999. https://doi.org/10.1016/j.tws.2020.106999.

Lieu, Q.X., Lee, D., Kang, J. and Lee, J. (2019), "NURBS-based modeling and analysis for free vibration and buckling problems of in-plane bi-directional functionally graded plates", *Mech. Adv. Mater. Struct.*, **26**(12), 1064-1080. https://doi.org/10.1080/15376494.2018.1430273.

Lieu, Q.X., Lee, S., Kang, J. and Lee, J. (2018), "Bending and free vibration analyses of in-plane bi-directional functionally graded plates with variable thickness using isogeometric analysis", *Compos. Struct.*, **192**, 434-451. https://doi.org/10.1016/j.compstruct.2018.03.021.

Mehrabadi, S.J. and Aragh, B.S. (2013), "On the thermal analysis of 2-D temperature-dependent functionally graded open cylindrical shells", *Compos. Struct.*, **96**, 773-785. https://doi.org/10.1016/j.compstruct.2012.09.036.

Molla-Alipour, M., Shariyat, M. and Shaban, M. (2020), "Free vibration analysis of bidirectional functionally graded conical/cylindrical shells and annular plates on nonlinear elastic foundations, based on a unified differential transform analytical formulation", *J. Solid Mech.*, **12**(2), 385-400. https://doi.org/10.22034/JSM.2019.1869981.1450.

Nemat-Alla, M. (2003), "Reduction of thermal stresses by developing two-dimensional functionally graded materials", *Int. J. Solids Struct.,* **40**(26), 7339-7356. https://doi.org/10.1016/j.ijsolstr.2003.08.017.

Pradyumna, S. and Bandyopadhyay, J.N. (2008), "Free vibration analysis of functionally graded curved panels using a higher-order finite element formulation", *J. Sound Vib.*, **318**(1-2), 176-

92. https://doi.org/10.1016/j.jsv.2008.03.056.
Punera, D. and Kant, T. (2017), "Free vibration of functionally graded open cylindrical shells based on several refined higher order displacement models", *Thin-Walled Struct*., **119**, 707-726. https://doi.org/10.1016/j.tws.2017.07.016.
Ramteke, P.M., Panda, S.K. and Nitin, S> (2019), "Effect of grading pattern and porosity on the eigen characteristics of porous functionally graded structure", *Steel Compos. Struct*., **33**(6), 865-875. https://doi.org/10.12989/scs.2019.33.6.865.
Ramteke, P.M. and Panda, S.K. (2021), "Free vibrational behaviour of multi-directional porous functionally graded structures", *Arab. J. Sci. Eng*., **46**(8), 7741-7756. https://doi.org/10.1007/s13369-021-05461-6.
Ramteke, P.M., Panda, S.K. and Patel, B. (2022), "Nonlinear eigenfrequency characteristics of multi-directional functionally graded porous panels", *Compos. Struct.*, **279**, 114707. https://doi.org/10.1016/j.compstruct.2021.114707.
Sah, S.K. and Ghosh, A. (2022), "Influence of porosity distribution on free vibration and buckling analysis of multi-directional functionally graded sandwich plates", *Compos. Struct.*, **279**, 114795. https://doi.org/10.1016/j.compstruct.2021.114795.
Salehipour, H., Nahvi, H. and Shahidi, A.R. (2015), "Exact closed-form free vibration analysis for functionally graded micro/nano plates based on modified couple stress and three-dimensional elasticity theories", *Compos. Struct.*, **124**, 283-291. https://doi.org/10.1016/j.compstruct.2015.01.015.
Salehipour, H. and Shahsavar, A. (2018), "A three-dimensional elasticity model for free vibration analysis of functionally graded micro/nano plates: Modified strain gradient theory", *Compos. Struct.*, **206**, 415-424. https://doi.org/10.1016/j.compstruct.2018.08.033.
Salehipour, H., Shahsavar, A. and Civalek, O. (2019), "Free vibration and static deflection analysis of functionally graded and porous micro/nanoshells with clamped and simply supported edges", *Compos. Struct.*, **221**, 110842. https://doi.org/10.1016/j.compstruct.2019.04.014.
Salehipour, H., Shahgholian-Ghahfarokhi, D., Shahsavar, A., Civalek, O. and Edalati, M. (2022), "Static deflection and free vibration analysis of functionally graded and porous cylindrical micro/nano shells based on the three-dimensional elasticity and modified couple stress theories", *Mech. Based Des. Struct. Mach.*, **50**(6), 2184-2205. https://doi.org/10.1080/15397734.2020.1775095.
Sayyad, A.S. and Ghugal, Y.M. (2021), "Static and free vibration analysis of doubly-curved functionally graded material shells", *Compos. Struct.*, **269**, 114045. https://doi.org/10.1016/j.compstruct.2021.114045.
Sharma, N., Tiwari, P., Maiti, D.K. and Maity, D. (2021), "Free vibration analysis of functionally graded porous plate using 3-D degenerated shell element", *Compos. Part C: Open Access*, **6**, 100208. https://doi.org/10.1016/j.jcomc.2021.100208.
Şimşek, M. (2015), "Bi-directional functionally graded materials (BDFGM) for free and forced vibration of timoshenko beams with various boundary conditions", *Compos. Struct*., **133**, 968-78. https://doi.org/10.1016/j.compstruct.2015.08.021.
Sobhy, M. and Zenkour, A.M. (2019), "Porosity and inhomogeneity effects on the buckling and vibration of double-fgm nanoplates via a quasi-3d refined theory", *Compos. Struct*., **220**, 289-303. https://doi.org/10.1016/j.compstruct.2019.03.096.
Tahouneh, V. and Naei, M.H. (2016), "The effect of multi-directional nanocomposite materials on the vibrational response of thick shell panels with finite length and rested on two-parameter elastic foundations", *Int. J. Adv. Struct. Eng*., **8**(1), 11-28. https://doi.org/10.1007/s40091-016-0110-4.
Talebizadehsardari, P., Salehipour, H., Shahgholian-Ghahfarokhi, D., Shahsavar, A. and Karimi, M. (2022), "Free vibration analysis of the macro-micro-nano plates and shells made of a material with functionally graded porosity: A closed-form solution", *Mech. Based Des. Struct. Mach.*, **50**(3), 1054-1080. https://doi.org/10.1080/15397734.2020.1744002.
Tornabene, F. (2009), "Free vibration analysis of functionally graded conical, cylindrical shell and annular plate structures with a four-parameter power-law distribution", *Comput. Method. Appl. M.*, **198**(37-40), 2911-2935. https://doi.org/10.1016/j.cma.2009.04.011.
Tornabene, F., Viola, E. and Inman, D.J. (2009) "2-D differential quadrature solution for vibration analysis of functionally graded conical, cylindrical shell and annul plate structures", *J. Sound Vib.*, **328**(3), 259-290. https://doi.org/10.1016/j.jsv.2009.07.031.
Wu, C.P. and Yu, L.T. (2019), "Free vibration analysis of bi-directional functionally graded annular plates using finite annular prism methods", *J. Mech. Sci. Tech.*, **33**(5), 2267-2279. https://doi.org/10.1007/s12206-019-0428-5.

CC